EFFECT OF GRAPHENE NANOPLATELETS THICKNESS ON STRAIN SENSITIVITY OF NANOCOMPOSITES: A DEEPER THEORETICAL TO EXPERIMENTAL ANALYSIS

M. Sanchez[a], R. Moriche[a,b], Xoan F. Sánchez-Romate[a,c,*], S.G. Prolongo[a], J. Rams[a], A. Ureña[a]

[a]Materials Science and Engineering Area, University Rey Juan Carlos, C/Tulipán s/n, Móstoles, 28933, Madrid, Spain

bDepartamento de Ingeniería y Ciencia de los Materiales y del Transporte, Universidad de Sevilla, Avda. Camino de los Descubrimientos, s/n, 41092 Sevilla, Spain

[c]Department of Aerospace Materials and Manufacturing Process, Escuela Técnica Superior de Ingeniería Aeronáutica y del Espacio, Universidad Politécnica de Madrid, Plaza Cardenal Cisneros 3, 28040, Madrid, Spain

Corresponding author: * xoan.fernandez.sanchezromate@urjc.es

Abstract

Conductive epoxy nanocomposites were prepared using two different thickness graphene nanoplatelets (GNPs) as reinforcement, H25 and M25. In both cases, 3 and 5 wt. % GNPs was dispersed into the matrix by means of sonication and calandering processes. The piezoresistive mechanisms of these GNPs/epoxy sensors were studied under tensile and flexural tests. Under tensile loads, H25 nanocomposites, with 15 nm thickness, have a lower sensitivity at low strains and higher at high strains than M25 ones, with 6 nm thickness. This apparently anomalous behavior is explained under the basis of a theoretical model where two types of contacts between GNPs are considered. H25 nanocomposites

show a prevalence of type I tunneling mechanisms at low strains and a prevalence of type II contacts at high strains, explaining this more pronounce exponential effect of the electrical resistance. In case of flexural tests, tensile and compressive subjected faces were monitored separately. Lower values of sensitivity than in tensile tests were observed due to the influence of breakage and creation of electrical pathways, showing a similar trend at low and high strains for H25 and M25 nanocomposites.

Keywords: A. Nano composites; A. Smart materials; B. Electrical properties; C. Modelling

1. Introduction

Carbon-based nanomaterials, especially carbon nanotubes (CNTs) and graphene, have gathered exceptional interest during the last decade due to their extraordinary mechanical, electrical and thermal properties, high surface area, chemical sensitivity, flexibility, transparency, etc. [1,2]. More specifically, their addition into insulator matrix induces the creation of conductive networks making them electrically conductive [3,4]. Therefore, these carbon allotropes can be used in a wide range of smart materials developed for practical applications in advanced aerospace, mechanical parts, energy technology, bionics and medical technologies [5,6]. There is also an interest in structural health monitoring (SHM) applications for which conductive polymer composites are considered in order to replace traditional sensors in certain applications due to their flexibility and ease of processing. Their use allows avoiding some of the limitations that traditional strain sensors have, such as they are discrete point, fixed directional, not flexible and separated from the material or structure that is monitored [7].

In these materials, the conductive networks formed through the polymer are very sensitive to strain or damage, even at low loads. Theoretical and experimental studies have been carried out to find out the working mechanisms of this new type of strain sensor based on CNT-polymer [8-12] and graphene–polymer [13-16] composites, proving the high potential and applicability of graphene-based nanocomposites leading to impressive values of sensitivity of around 30-70 [17] and demonstrating their use in a wide range of applications

such as in stretchable sensors in combination with other nanoparticles [18] or by using them as fiber coating in multiscale glass-fiber composites [19]. In general, the mechanical and self-sensing performances of the polymer composites depend on the intrinsic features of carbon particles including their morphology (dimension, aspect ratio) as well as on their distribution and alignment within the polymeric matrix [20-23]. In fact, it has been proved that graphene-based nanocomposites show much higher percolation threshold, that is, the critical volume fraction in which a material becomes electrically conductive than carbon nanotube-based ones, leading from 2-5 wt. % values to CNT contents below 0.1 wt. % [24-26]. In this context, there are several studies also devoted to the analysis of the tunneling mechanisms and their modeling [27,28]. Besides, the surface treatment of particles, such as metal coatings or functionalization, has influence on the sensitivity of this type of sensors [29,30].

For this reason, this work aims to further investigate on the main parameters that could affect the sensitivity of GNP/epoxy systems, by developing a novel theoretical model taking the geometry and possible interactions between nanoparticles into account. This would explain some possible anomalous behaviors and would give enough information to select the proper nanoparticle geometry and dispersion procedure. In our current research, two GNPs with different thickness (6 and 15 nm) were used for the fabrication of GNP/epoxy nanocomposites from mixtures obtained dispersing GNPs by sonication and calandering. Firstly, the structural characterization of base materials and

GNP/epoxy nanocomposites was comparably investigated in detail. Secondly, electrical sensitivity of these strain sensors was analyzed under tensile and flexural tests. The deformation evolution and *in situ* electrical resistance response during loading were analyzed and a simple theoretical model, based on other studies for CNTs [31] was developed in order to get a deeper knowledge about the influence of the geometry of GNPs on tunneling mechanisms inside the nanocomposites. Taking into account that in flexural tests the samples are subjected to tensile and flexural loads, the results from flexural test were compared with the uniaxial loading ones. Finally, the sensitivity of sensors was correlated with GNPs distribution in the epoxy matrix, which was influenced by the thickness of the nanoplatelets.

2. Experimental

2.1. Materials

The fabrication of GNP/epoxy nanocomposites was made with an epoxy resin obtained from a basic DGEBA monomer (*Araldite LY556*) cured with an aromatic amine (*Araldite XB3473*). Two types of GNPs provided by *XGScience* were used: i) GNPs powder grade M, with an average thickness of 6 nm and an average lateral size of 25 μm (referred as M25), and ii) GNPs powder grade H with an average thickness of 15 nm and an average lateral size of 25 μm (referred as H25). The electrical conductivity data supplied by the manufacturer are similar for both GNPs, ~10^7 S/m parallel to the surface and ~10^2 S/m in the

perpendicular direction. The main properties of M and H grade particles are summarized in Table 1.

2.2. GNP/epoxy nanocomposites fabrication

Nanocomposites with 3 and 5 wt. % GNPs using powders with H grade were manufactured and compared to M grade from previous studies [16]. The contents were selected to be near percolation threshold, determined around 2 wt. %. GNPs were dispersed in the monomer by (1) sonication followed by (2) calandering which consisted in three steps. The conditions were optimized in previous studies [32] and are summarized in Table 2.

Afterwards, the GNP/epoxy mixtures were degassed under vacuum at 80 °C for 15 minutes to remove dissolved air. Finally, the hardener was added in a stoichiometric weight ratio 100:23 (monomer:hardener) and the mixture was cured at 140 °C for 8 hours. To identify the samples, the following code was used: Resin (LY), wt. % and type of GNPs.

2.3. GNP/epoxy nanocomposites characterization

The electrical conductivity of nanocomposites doped with different types of GNPs was measured. DC volume conductivity was evaluated according to ASTM D257 using a *Source Meter Unit* instrument (*KEITHLEY 2410*). The electrical resistance was determined by calculating the slope of the current–voltage characteristic curve within the range of 0-15 V and three samples (10 × 10 × 1 mm^3) were tested per each nanocomposite. The dispersion of

nanoreinforcement in the matrix was evaluated from the analysis of the fracture surfaces of flexural tests by Scanning Electron Microscopy (SEM) using an apparatus *Hitachi 3400*. Additionally, Transmission Electron Microscopy (TEM), *Philips 200*, was used to corroborate the thickness of the GNPs.

2.4. Structural health monitoring tests

For the monitoring tests, two copper electrodes were attached to the sample surface using conductive silver paint to minimize the contact resistance. Electrodes were placed on composites using different configurations depending on the mechanical test (tensile or flexural), as shown in Figure 1. In tensile tests, electrodes were placed forming two rings with a separation of 30 mm (Figure 1a) in 6 samples with dimensions according to the ASTM D638 with a thickness of 4 mm. Configurations under flexural test are shown in Figures 1b and 1c in a sample with dimensions 60 × 12.7 × 1.7 mm^3 following ASTM D790. In the first case, contacts were placed in the lower side between the two cylinders with a separation of 14 mm (Figure 1b), where the material is mainly subjected to compression loads (3 samples were tested). The second configuration used in flexural test consisted in locating the electrodes on the top side (4 samples were tested), where only one flexural cylinder is placed, maintaining the same distance of 14 mm, and where tensile loads prevail (Figure 1c).

Tensile and flexural tests were performed in a *MTS Alliance RF/100* synchronized with the electrical measurements. For each configuration, electrical resistance was evaluated and recorded by an *Agilent 34410A*. The initial resistance between contacts was measured and its change was recorded by using the following equation:

$$R_N = \frac{R - R_0}{R_0} = \frac{\Delta R}{R_0} \quad (1)$$

Where R is the measured electrical resistance at an instant and R_o is the initial electrical resistance of the nanocomposite for the chosen contact configuration. The corresponding sensitivity (gauge factor) of the samples was calculated as the relationship between the normalized resistance (R_N) and strain (ε) according to the following expression:

$$S = \frac{R_N}{\varepsilon} \quad (2)$$

However, due to the exponential effect of tunneling resistance, it is more interesting to define the sensitivity as the derivative of the normalized resistance divided by the strain:

$$S = \frac{dR_N}{d\varepsilon} \quad (3)$$

3. Results and discussion

3.1. Structural characterization of base materials and GNP/epoxy nanocomposites

The morphology of the as-received GNPs powders was studied by SEM and TEM (Figure 2). The lateral size of both powders varied from 10 to 100 μm. The difference indicated by the manufacturer was the higher number of graphene layers of the H25 particles. It was observed that as the number of graphene layers of GNPs increases: (i) the number of graphene particles incorporated into the matrix and (ii) the folding tendency decrease. GNPs tend to restack due to their large van der Waals and strong π-π interactions and this is the reason why H25 particles keep together [33].

In both cases, after the sonication-calandering process, a homogenous distribution of the nanoparticles was achieved as it is shown in the fracture surfaces after flexural tests (Figures 3a and 3c). In both materials, there were clean flat zones where GNPs have not been observed. The fracture mechanism was brittle in the regions free from GNPs and river marks were formed in the resin. That is characteristic of brittle fracture and river marks were mainly localized in the vicinity of GNPs.

The brittle zones in the LY3M25 (Figure 3a) were smaller (about less a third in lateral size) than those in the LY3H25 one (Figure 3c). This indicates that the number of nanoparticles effectively incorporated into the matrix was much higher for the LY3M25 nanocomposite than for the LY3H25, as expected,

because of a lower thickness of M25 GNPs. The homogeneous distribution of flat zones indicates that the particle distribution was adequate in both cases. At higher magnification, it was possible to find folded M25 particles (arrowed zone in Figure 3b); while in the case of H25 GNPs the particles observed were mainly flat and stacked, like in as received condition (Figure 3d).

The electrical conductivity measured for the nanocomposites is listed in Table 3. The conductivity of materials doped with M25 GNPs is lower than those reinforced with H25 ones. Conductivity in carbon-based nanomaterials can be due to two different mechanisms: 1) contact between conductive particles and 2) electron tunneling between them. In the last mechanism, the interparticle separation is in the order of nanometers. To explain the obtained conductivity values, the morphology and the effective number of the nanoparticles in the matrix have to be also taken into account. The M25 nanoplatelets have a higher aspect ratio, about 2.5 times H25 particles. However, the nanocomposite reinforced with M25 is less piled up graphene nanoplatelets and they show a higher entanglement causing a detriment in the electrical properties and a

reduction on their effective aspect ratio. This reduction induces an increase of the percolation threshold, that is, the volume fraction of GNPs where the material becomes electrical conductivity [34]. The combination of these effects would explain the lower electrical conductivity of M25 nanocomposites [34,35].

3.2. Monitoring tests under tensile conditions

Tensile tests of both nanocomposites were performed, and the variation of electrical resistance was measured simultaneously. The results of the electrical behavior obtained from tensile tests for both nanocomposites are shown in Figure 4. The fracture of these materials was brittle and a sharp jump in the resistance was registered at the end of the tests when the fracture propagated. The shape of the loading curves for both nanocomposites was similar.

It is observed that electrical resistance increases with applied strain, as expected due to the separation between adjacent nanoparticles during the test.

This change in the electrical resistance is more pronounced at higher strain rates, showing a clear exponential behavior.

In case of elastic deformation with strain values below 0.005, a linear relationship between resistance and strain can be obtained with a correlation factor, $R^2 = 0.999$, in both cases. The gauge factor calculated in the initial linear behavior was 13 ± 3, 12 ± 2 and 8 ± 4, and 7 ± 5 for the LYM25 and LYH25 nanocomposites at 3 wt. % and 5 wt. %, respectively. Considering that the traditional metal-foils strain gauges have factors of around 2, with these GNP/epoxy nanocomposites the sensitivity increases up to the order of 6-fold. When comparing to CNT nanocomposites, with gauge factors around 2-3 [26], they also show a very significant sensitivity, so they would have many practical applications for strain sensing.

At higher deformations, the sensitivity (S') significantly increased for both nanocomposites reaching values of 33 ± 7, 28 ± 5 and 65 ± 10 and 55 ± 12 at strain values ~0.025 for tested LYM25 and LYH25 nanocomposites at 3 wt. % and 5 wt. %, respectively. Therefore, the maximum sensitivity achieved in these systems was 65 ± 10 for LYH25 at 3 wt. %, which nevertheless shows the minor sensitivity at low strain. In addition to that, sensitivity decreases with GNP content, as expected, due, at first sight, to a lower prevalence of tunneling mechanisms.

These results could be surprising at a first sight due to the higher-lower sensitivity of H25 and M25 nanocomposites depending on the strain level and on the GNP content, so it is necessary to go deeper into sensing mechanisms.

3.2.1 Modeling of nanocomposite tunneling mechanisms at tensile state A theoretical model is developed based on other theoretical studies of electromechanical properties proposed for carbon nanotubes (CNTs) [31].

It is widely known that the main conducting mechanisms are due to the tunneling effect between adjacent nanoparticles. Electrical resistance due to this effect is calculated by applying the following formula:

$$R_{tunnel} = \frac{h^2 t}{Ae^2\sqrt{2m\varphi}} \exp\left(\frac{4\pi t}{h}\sqrt{2m\varphi}\right) \quad (4)$$

Where *A* is the tunneling cross-sectional area, *e* and *m* are the electron charge and mass, respectively, *h is* the Planck's constant, *φ is* the height barrier of the epoxy and *t is* the tunneling distance.

Based on Y. Kuronuma et. al. [31] study for CNTs, the GNPs interaction can be divided in two types, as observed in the schematics of Figure 5: type I, based on the tunneling effect out of plane due to the overlap between GNPs and type II, based on the conventional tunneling effect in plane. Therefore, the electrical resistance would be divided in two different terms:

$$R_I = \frac{h^2 t_I}{A_I e^2 \sqrt{2m\varphi}} \exp\left(\frac{4\pi t_I}{h}\sqrt{2m\varphi}\right) \quad (5)$$

$$R_{II} = \frac{h^2 t_{II}}{A_{II} e^2 \sqrt{2m\varphi}} \exp\left(\frac{4\pi t_{II}}{h}\sqrt{2m\varphi}\right)$$

Where the subscript *I* and *II* denote the type I and II GNPs contacts, respectively.

Tunneling distance for type I and II is calculated from the total strain of the nanocomposite depending on the Poisson effects:

$$t_I = (1 - v\varepsilon)t_{IO}^M$$
$$t_{II} = (1 + \varepsilon)t_{IIO}^M \quad (6)$$

Where v is the Poisson modulus of the matrix, and ε is the total strain of the nanocomposite. The subscript 0 denotes the initial condition, that is, the initial tunneling distance.

The initial tunneling distance can be calculated from the volume fraction of the GNPs by applying a power law [31]:

$$t_{IO}^{M} = t_{IIO}^{M} = \alpha(v_G)^{\beta} \quad (7)$$

Where the parameters α and β are calculated from the value of the tunneling distance at percolation threshold, that is, the point where the material becomes conductive by creating percolating paths; and the value at maximum content, which coincides with the Van der Waals distance of 0.34 nm.

In addition to that fact, it is necessary to estimate the tunneling areas for the type I and II contacts, A_I and A_{II}.

A_{II} is estimated as the average contact of two GNP cross-sectional areas, that is $A_{II} = db/2$; where d is the average lateral size of the GNPs and b the average thickness. A_I depends on the effective area of the GNPs. It implies that more entangled GNPs will have less contact area than those more stretched, as observed in the schematics of Figure 6.

Total electrical resistance R_T, thus, can be calculated as a fraction of resistance due to type I and II contacts, respectively. That is:

$$R_T = (1 - f)R_I + fR_{II} \quad (8)$$

Therefore, the change of the normalized resistance will be:

$$\frac{\Delta R}{R_0} = \frac{R_T - R_{T0}}{R_{T0}} \quad (9)$$

Being R_T and R_{T0} the values of the total resistance at applied strain and at initial state respectively.

The sensitivity at a strain, S_i, will be calculated, thus, as follows:

$$S_i = \frac{d\left(\frac{\Delta R}{R_0}\right)}{d\varepsilon} = \frac{\left(\frac{\Delta R}{R_0}\right)_i - \left(\frac{\Delta R}{R_0}\right)_{i-1}}{\varepsilon_i - \varepsilon_{i-1}} = \frac{\frac{R_{Ti} - R_{T0}}{R_{T0}} - \frac{R_{Ti-1} - R_{T0}}{R_{T0}}}{\varepsilon_i - \varepsilon_{i-1}} = \frac{\frac{R_{Ti} - R_{Ti-1}}{R_{T0}}}{\varepsilon_i - \varepsilon_{i-1}} \quad (10)$$

Tunneling distance calculated by Equation (7) will be higher in M25 nanocomposites due to a higher percolation threshold explained by its lower effective aspect ratio [36]

3.2.2 Analysis of the piezoresistive response of nanocomposites based on the model

Figure 7 shows the calculated *S* by applying Equation (10) at strain levels ranging from 0 to 0.03 depending on the contact area of type I and the overlap factor, *f*.

It can be observed that A_I has a strong influence on the sensitivity of nanocomposites. Low contact areas, that is, a higher entanglement, implies a severe reduction of the sensitivity due to a predominance of tunneling mechanisms by type I. This is explained because of a higher R_I and, thus, a predominance over the total resistance. In fact, it is possible to achieve negative sensitivities if the contact regions of type I are too small.

Moreover, it is observed that *f* has a prevalent influence on the sensitivity of nanocomposites. Higher values *f* denotes a prevalence of type II contacts in the total resistance, that is, a higher sensitivity. On the other hand, when *f* is too low, the main tunneling mechanisms are due to type I contacts, implying a lower (even negative) sensitivity.

Therefore, by adjusting these parameters, it is possible to justify the changes in the trend of the sensitivity for H25 and M25 nanocomposites.

Figure 8 shows the variation of the normalized electrical resistance as a function of strain for the H25 and M25 nanocomposites by adjusting the model parameters to the experimental results. The *f* value is set as 0.19 for M25 and 0.0055 for H25, that is, there are more overlapping points in H25 than in M25 nanocomposites. In addition to that fact, A_I is lower for M25 nanocomposites (10 vs 325 μm^2 in H25 nanocomposites at 3 wt. % and 20 vs 800 μm at 5 wt. %). The reduction in the tunneling area implies, as commented before, a higher entanglement (Figure 6) as expected due to the higher aspect ratio of M25

GNPs. This leads to a higher effective area of H25 GNPs, implying a prevalence of type I contacts over the prevalence of type II contacts in M25 nanocomposites. Moreover, at higher contents, there are more nanoparticles inside the nanocomposite, so there can be more conducting paths between GNPs and, thus, leading to an increase of tunneling area.

At both contents, by analyzing the sensing curve, it can be noticed that at low strain levels there are a higher prevalence of type I conducting mechanisms in H25 nanocomposites while at high strain levels in H25 nanocomposites the effect of their effective area is more prevalent than in M25, so the total electrical resistance is more influenced by the prevalence of type II conducting mechanisms as the electrical resistance of this type of contacts is much higher than the type I and therefore, the changes of the total resistance are more influenced by the in-plane contacts. Therefore, by simple theoretical calculations, the electrical behavior of GNP nanocomposites at tensile loads can be better understood.

3.3 Monitoring tests under flexural conditions

The electrical behavior of LY3M25 and LY3H25 nanocomposites under flexural deformation was also measured. In this case, in different tests the electrical contacts were located on the compression or on the tensile subjected sides of the samples. The corresponding stress-strain and sensing curves are shown in Figures 9 and 10, respectively. A common characteristic to both nanocomposites is that the electrical response presented a nearly linear

tendency. Changes of sensitivity depending on the applied strain elucidate the exponential character of the electrical curve.

At low strain values, ε~0.005, the sensitivity values were 2.0 ± 0.7, 2.1 ± 0.8 and 1.2 ± 0.7 and 2.0 ± 0.3 for LYM25 and LYH25 at 3 and 5 wt. %, respectively, respectively when the compression side was monitored. At high strain values, ε~0.025, the sensitivity increased up to 4.6 ± 1.1, 4.8 ± 0.4 and 4.4 ± 0.4 and 4.3 ± 0.7, respectively. Different values were obtained in the case of the tensile subjected side: at low strain sensitivities were 3.4 ± 0.7, 3.0 ± 0.5 and 3.3 ± 0.3 and 4.9 ± 1.1 while at high strain they were 7 ± 1, 6 ± 1 and 9 ± 1 and 6.0 ± 0.5 for M25 and H25-GNPs, respectively.

The increase of electrical resistance, shown in Figure 10, indicates that the dominant mechanism that takes place is the breakage of the conductive network regardless of the location of the contacts on the top (compressive surface) or bottom (tensile surface) of the sample.

These changes of the electrical response, i.e. sensitivity, when samples are tested in tensile and flexural modes are attributed to the geometry of the test. It is important to note that the electrical signal measured during the test is influenced by a certain volume of the sample. This volume could include some tensile subjected areas which, in combination to the breakage of electrical pathways due to buckling effects, would explain the positive sensitivity at compression side, as reported in other studies for CNTs [37].

To understand the different sensitivities achieved for M25 and H25 GNPs it is necessary to understand the effect of rearrangement of nanoparticles during compressive tests previously reported by Wang *et al.* in the study of carbon nanotube filled silicone rubber nanocomposites under compressive loads [38]. This phenomenon induces the creation of new electrical pathways and occurred more significantly in H25 GNPs where the number of conductive paths is reduced. Because of this fact, the value of the sensitivity is smaller than in the tensile tests: due to a higher contribution of the new created electrical paths. The reduction of sensitivity at high strain values, taking tensile tests sensitivity as reference, was in the order of ~ 86 % and ~ 93 % for M25 and H25 doped matrices (compressive subjected face in flexural – uniaxial tensile test), respectively, what elucidates the mentioned influence.

The sensitivity of the tensile subjected surface in flexural tests also decreased compared to that of uniaxial tensile tests. The reduction of the sensitivity obtained is attributed to the effect of the volume of influence, including some areas near the neutral axis and even, the compression side, inducing a reduction of the sensitivity [37]. The reduction in this case was less pronounced since a minor number of conductive paths are created in influence area affecting the tensile side reaching a reduction of ~ 79 % and ~ 86 % when using M25 and H25 GNPs, respectively. Those values show again a lower sensitivity of H25 particles at low strains and a higher sensitivity at high strains in a similar way than in pure tensile tests.

Calculated sensitivity values for tensile and flexure are summarized in Figure 11. Due to the exponential character of the electrical response, sensitivity values at low strain (Figure 11a) were lower than those measured at higher strain values (Figure 11b) for all tested configurations. Although obtained sensitivity at low strain values was considerably lower, it was in the range of commercial metal-foils strain gauges. The maximum gauge factor around 65 was registered during the application of uniaxial loads in tensile tests at high strain values.

Conclusions

The sensitivity of GNP/epoxy piezoresistive strain sensors reinforced with nanoplatelets with different thicknesses was evaluated. The influence of the morphology and the effective number of nanoparticles in the resin on the electrical conductivity and, consequently, on the sensitivity of the sensor was elucidated.

When the same weight content of GNPs is used as reinforcement, high thickness nanoplatelets involve a lower number of particles into the resin. However, these particles remain flat after the dispersion process, avoiding wrinkled structures, providing a higher electrical conductivity. The reported sensitivities show a more accused exponential behavior in case of H25 nanoparticles with lower sensitivity than M25 at low strain levels and higher at high strain levels.

A theoretical model is proposed to better understand how geometry of nanofiller can affect the tunneling mechanisms and, thus, the sensitivity. It shows that a lower entanglement leads to a higher sensitivity as well as a more prevalence of in-plane contacts. Therefore, the lower to higher sensitivities at low-high strain levels of H25 is explained by a prevalence of overlapping mechanisms at low strain levels and a prevalence of its higher effective area at high strains due to this lower entanglement.

Samples tested in a flexural mode showed a reduced sensitivity. The reduction on this property, compared to that obtained in uniaxial tensile tests, is attributed to the creation of new electrically conductive paths favored by the bending configuration simultaneous to the network breakage due to buckling mechanisms and some tensile influenced area. This apparent reduction on the sensitivity is more pronounced in samples reinforced with higher thickness GNPs because the creation of new conductive paths has more impact in the electrical properties. Consequently, these samples are more sensitive to changes in the electrical network due to the lower number of GNPs into the matrix.

Acknowledgements

The authors would like to acknowledge the Ministerio de Economía y Competitividad of Spain Government (Project MAT2016-78825-C2-1-R) and Comunidad de Madrid Government (P2013/MIT-2862). In addition, the authors would like to thank Dr. M. J. Sayagués from Instituto de Ciencia de Materiales

de Sevilla, for the TEM images.

References

1. Robertson J. Growth of nanotubes for electronics. Materials Today 2007;10(1):36-43.

2. Geim AK, Novoselov KS. The rise of graphene. Nature Materials 2007;6(3):183-191.

3. Monti M, Rallini M, Puglia D, Peponi L, Torre L, Kenny JM. Morphology and electrical properties of graphene–epoxy nanocomposites obtained by different solvent assisted processing methods. Composites Part A: Applied Science and Manufacturing 2013;46:166-172.

4. Mostaani F, Moghbeli MR, Karimian H. Electrical conductivity, aging behavior, and electromagnetic interference (EMI) shielding properties of polyaniline/MWCNT nanocomposites. J Thermoplast Compos Mater 2018;31(10):1393-1415.

5. Hwang S, Park HW, Park Y, Um M, Byun J, Kwon S. Electromechanical strain sensing using polycarbonate-impregnated carbon nanotube–graphene nanoplatelet hybrid composite sheets. Composites Sci Technol 2013;89:1-9.

6. DeGraff J, Liang R, Le MQ, Capsal J, Ganet F, Cottinet P. Printable low-cost and flexible carbon nanotube buckypaper motion sensors. Materials & Design 2017;133:47-53.

7. Knite M, Tupureina V, Fuith A, Zavickis J, Teteris V. Polyisoprene—multi-wall carbon nanotube composites for sensing strain. Materials Science and Engineering: C 2007;27(5-8):1125-1128.

8. Hu N, Karube Y, Arai M, Watanabe T, Yan C, Li Y, Liu Y, Fukunaga H. Investigation on sensitivity of a polymer/carbon nanotube composite strain sensor. Carbon 2010;48(3):680-687.

9. Alamusi, Hu N, Fukunaga H, Atobe S, Liu Y, Li J. Piezoresistive Strain Sensors Made from Carbon Nanotubes Based Polymer Nanocomposites. Sensors 2011;11(11):10691-10723.

10. Sanli A, Benchirouf A, Mueller C, Kanoun O. Piezoresistive performance characterization of strain sensitive multi-walled carbon nanotube-epoxy nanocomposites. Sensors and Actuators A-Physical 2017;254:61-68.

11. Arif MF, Kumar S, Gupta TK, Varadarajan KM. Strong linear-piezoresistiveresponse of carbon nanostructures reinforced hyperelastic

polymer nanocomposites. Composites Part A: Applied Science and Manufacturing 2018;113:141-149.

12. Pu J, Zha X, Zhao M, Li S, Bao R, Liu Z, Xie B, Yang M, Guo Z, Yang W. 2D end-to-end carbon nanotube conductive networks in polymer nanocomposites: a conceptual design to dramatically enhance the sensitivities of strain sensors. Nanoscale 2018.

13. Zhao J, He C, Yang R, Shi Z, Cheng M, Yang W, Xie G, Wang D, Shi D, Zhang G. Ultra-sensitive strain sensors based on piezoresistive nanographene films. Appl Phys Lett 2012;101(6):063112.

14. Chiacchiarelli LM, Rallini M, Monti M, Puglia D, Kenny JM, Torre L. The role of irreversible and reversible phenomena in the piezoresistive behavior of graphene epoxy nanocomposites applied to structural health monitoring. Composites Sci Technol 2013;80:73-79.

15. Kumar SK, Castro M, Saiter A, Delbreilh L, Feller JF, Thomas S, Grohens Y. Development of poly (isobutylene-co-isoprene)/reduced graphene oxide nanocomposites for barrier, dielectric and sensingapplications. Mater Lett 2013;96:109-112.

16. Moriche R, Sanchez M, Jimenez-Suarez A, Prolongo SG, Urena A. Strain monitoring mechanisms of sensors based on the addition of graphene nanoplatelets into an epoxy matrix. Composites Sci Technol 2016;123:65-70.

17. Yang H, Yao X, Zheng Z, Gong L, Yuan L, Yuan Y, Liu Y. Highly sensitive and stretchable graphene-silicone rubber composites for strain sensing. Composites Science and Technology 2018;167:371-378.

18. Zhang F, Wu S, Peng S, Sha Z, Wang CH. Synergism of binary carbon nanofibres and graphene nanoplates in improving sensitivity and stability of stretchable strain sensors. Composites Science and Technology 2019;172:716.

19. Moriche R, Jiménez-Suárez A, Sánchez M, Prolongo SG, Ureña A. Graphene nanoplatelets coated glass fibre fabrics as strain sensors. Composites Science and Technology 2017;146:59-64.

20. Fu S, Feng X, Lauke B, Mai Y. Effects of particle size, particle/matrix interface adhesion and particle loading on mechanical properties of particulate– polymer composites. Composites Part B: Engineering 2008;39(6):933-961.

21. Ma P, Mo S, Tang B, Kim J. Dispersion, interfacial interaction and reagglomeration of functionalized carbon nanotubes in epoxy composites. Carbon 2010;48(6):1824-1834.

22. Oliva-Avilés A, Avilés F, Sosa V. Electrical and piezoresistive properties of multi-walled carbon nanotube/polymer composite films aligned by an electric field. Carbon 2011;49(9):2989-2997.

23. Cao X, Wei X, Li G, Hu C, Dai K, Guo J, Zheng G, Liu C, Shen C, Guo Z. Strain sensing behaviors of epoxy nanocomposites with carbon nanotubes under cyclic deformation. Polymer 2017;112:1-9.

24. Bauhofer W, Kovacs JZ. A review and analysis of electrical percolation in carbon nanotube polymer composites. Composites Sci Technol 2009;69(10):1486-1498.

25. Moriche R, Sanchez M, Prolongo SG, Jimenez-Suarez A, Urena A. Reversible phenomena and failure localization in self-monitoring GNP/epoxy nanocomposites. Composite Structures 2016;136:101-105.

26. Sánchez-Romate XF, Artigas J, Jiménez-Suárez A, Sánchez M, Güemes A, Ureña A. Critical parameters of carbon nanotube reinforced composites for structural health monitoring applications: Empirical results versus theoretical predictions. Composites Sci Technol 2019;171:44-53.

27. Wang W, Jayatissa AH. Computational and experimental study of electrical conductivity of graphene/poly(methyl methacrylate) nanocomposite using Monte Carlo method and percolation theory. Synth Met 2015;204:141-147.

28. Hashemi R, Weng GJ. A theoretical treatment of graphene nanocomposites with percolation threshold, tunneling-assisted conductivity and microcapacitor effect in AC and DC electrical settings. Carbon 2016;96:474-490.

29. Eswaraiah V, Balasubramaniam K, Ramaprabhu S. Functionalized graphene reinforced thermoplastic nanocomposites as strain sensors in structural health monitoring. Journal of Materials Chemistry 2011;21(34):1262612628.

30. Hu N, Itoi T, Akagi T, Kojima T, Xue J, Yan C, Atobe S, Fukunaga H, Yuan W, Ning H. Ultrasensitive strain sensors made from metal-coated carbon nanofiller/epoxy composites. Carbon 2013;51:202-212.

31. Kuronuma Y, Takeda T, Shindo Y, Narita F, Wei Z. Electrical resistancebased strain sensing in carbon nanotube/polymer composites under tension: Analytical modeling and experiments. Composites Sci Technol 2012;72(14):1678-1682.

32. Moriche R, Prolongo SG, Sánchez M, Jiménez-Suárez A, Sayagués MJ, Ureña A. Morphological changes on graphene nanoplatelets induced during dispersion into an epoxy resin by different methods. Composites Part B: Engineering 2015;72:199-205.

33. Li D, Müller MB, Gilje S, Kaner RB, Wallace GG. Processable aqueous dispersions of graphene nanosheets. Nature nanotechnology 2008;3(2):101.

34. Li J, Kim J. Percolation threshold of conducting polymer composites containing 3D randomly distributed graphite nanoplatelets. Composites Sci Technol 2007;67(10):2114-2120.

35. Sanchez-Romate XF, Jimenez-Suarez A, Sanchez M, Guemes A, Urena A. Novel approach to percolation threshold on electrical conductivity of carbon nanotube reinforced nanocomposites. Rsc Advances 2016;6(49):43418-43428.

36. Li J, Kim J. Percolation threshold of conducting polymer composites containing 3D randomly distributed graphite nanoplatelets. Composites Sci Technol 2007;67(10):2114-2120.

37. Sánchez-Romate XF, Moriche R, Jiménez-Suárez A, Sánchez M, Prolongo SG, Güemes A, Ureña A. Highly sensitive strain gauges with carbon nanotubes: From bulk nanocomposites to multifunctional coatings for damage sensing. Appl Surf Sci 2017;424:213-221.

38. Wang L, Wang X, Li Y. Relation between repeated uniaxial compressive pressure and electrical resistance of carbon nanotube filled silicone rubber composite. Composites Part A: Applied Science and Manufacturing 2012;43(2):268-274.

FIGURE CAPTIONS

Figure 1. Contact configurations used in tensile (a) and (b and c) flexural tests.

Figure 2. SEM images of as-received GNP powders grade (a, c) M and (b, d) H and TEM images of as-received GNP powders grade (e) M and (f) H.

Figure 3. SEM images of fractured surfaces of (a, b) LY3M25 and (c, d) LY3H25 after flexural tests (GNPs are arrowed).

Figure 4. Load-strain and resistance-strain curves of tensile tests of (a) LY3M25 (from R. Moriche et al. [16]), (b) LY3H25, (c) LY5M25 (from R. Moriche et al. [16]) and (d) LY5H25 nanocomposites.

Figure 5. Schematics of types of contact between adjacent GNPs in the nanocomposite.

Figure 6. Schematics of type I tunneling areas between GNPs indicating the reduction with entanglement.

Figure 7. Value of sensitivity as a function of (a) A_I and (b) f for a GNPs with a lateral size of 25 μm and a thickness of 6 nm.

Figure 8. Comparison between theoretical estimations and experimental results for M25 and H25 nanocomposites at (a) 3 and (b) 3 wt. % loading.

Figure 9. Load-strain and resistance-strain curves in the compression side of flexural tests of (a) LY3M25 (from R. Moriche et al. [16]), (b) LY3H25, (c) LY5M25 (from R. Moriche et al. [16]) and (d) LY5H25 nanocomposites.

Figure 10. Load-strain and resistance-strain curves in the tensile side of flexural tests of (a) LY3M25 (from R. Moriche et al. [16]), (b) LY3H25, (c) LY5M25 (from R. Moriche et al. [16]) and (d) LY5H25nanocomposites.

Figure 11. Sensitivity values obtained from flexural and tensile tests at (a) low and (b) high strain values (CS: Compression side, TS: Tensile side).

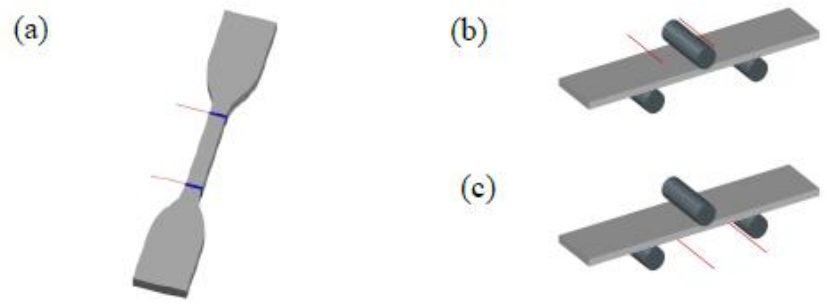

Figure 1.

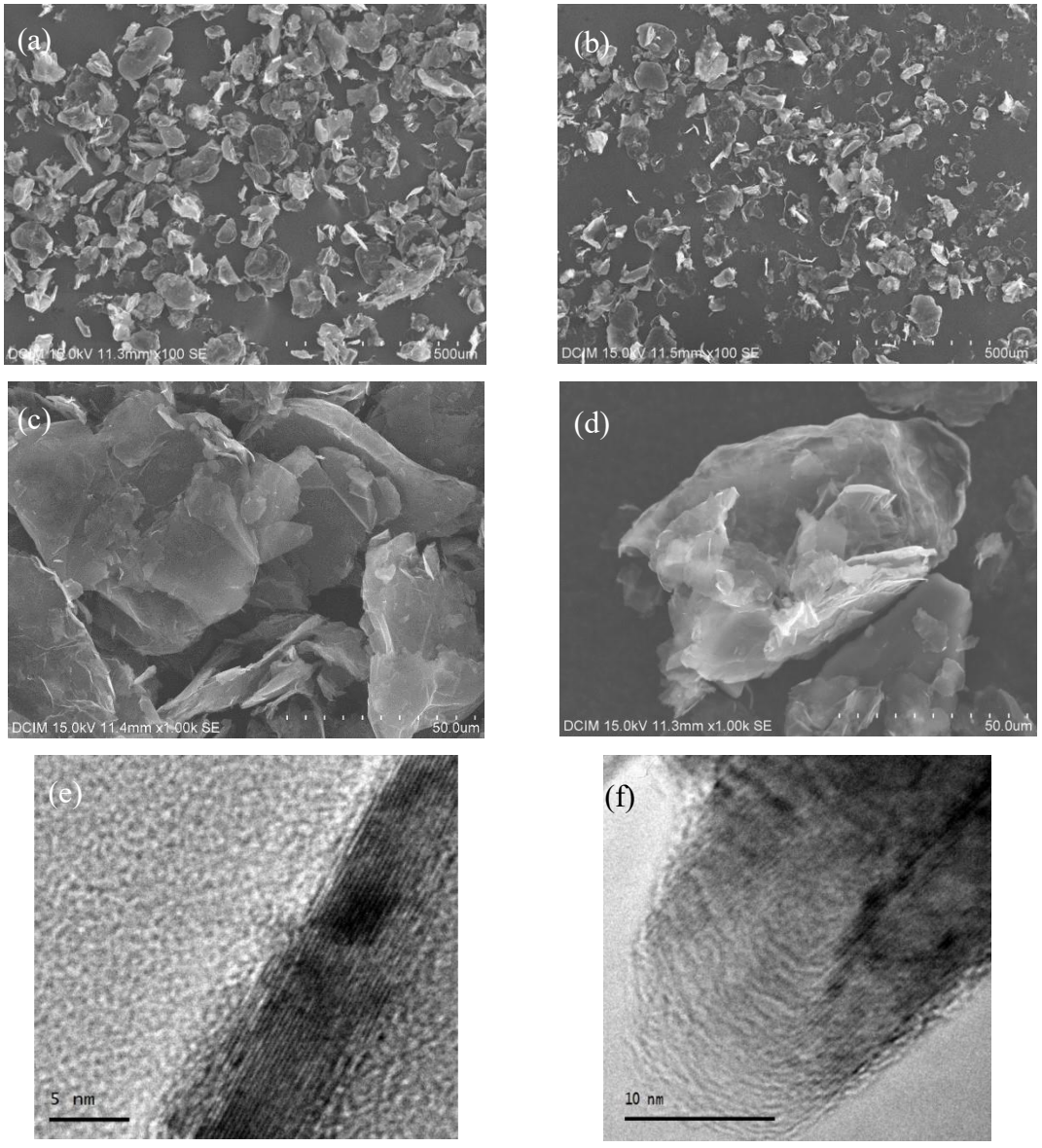

Figure 2.

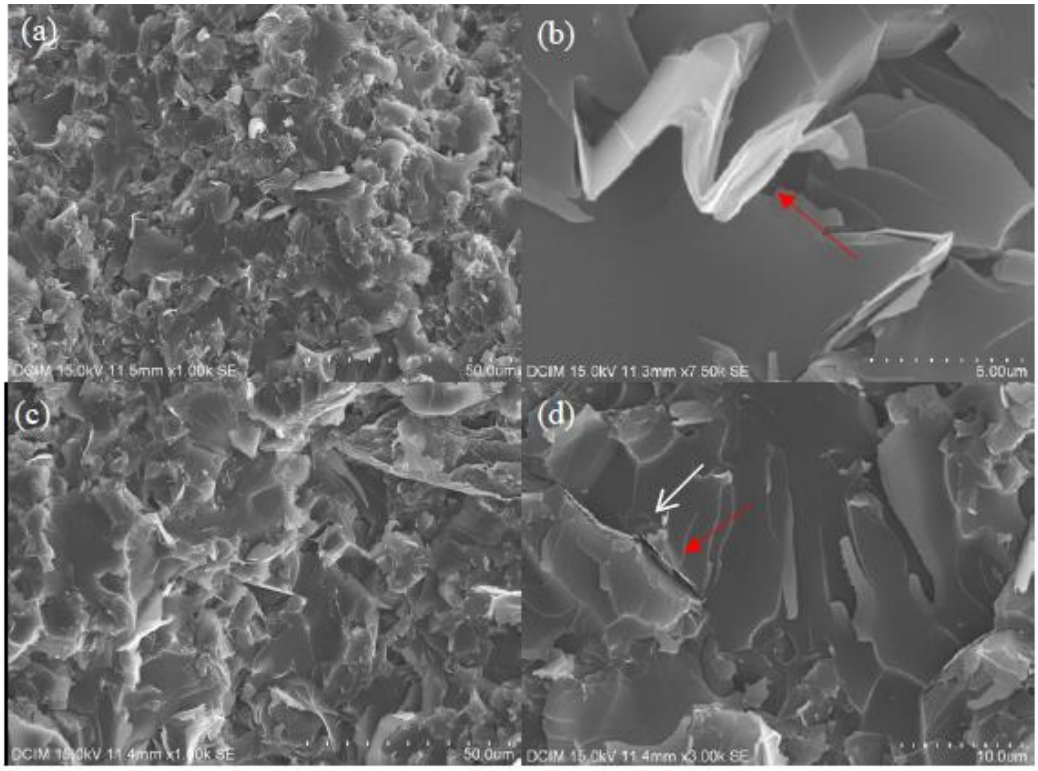
(a)
(b)
(c)
(d)
50.0um
5.00um
50.0um
10.0um

Figure 3.

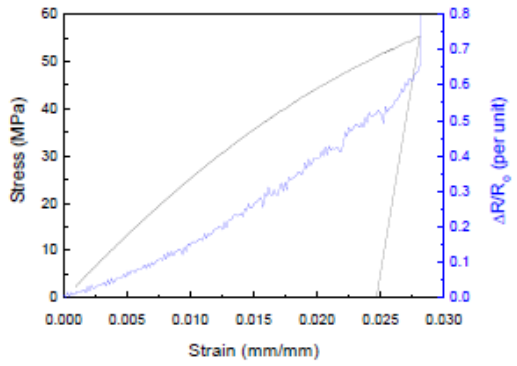
Stress (MPa)
ΔR/R0 (per unit)
Strain (mm/mm)
0.000
0.005
0.010
0.015
0.020
0.025
0.030

(a)

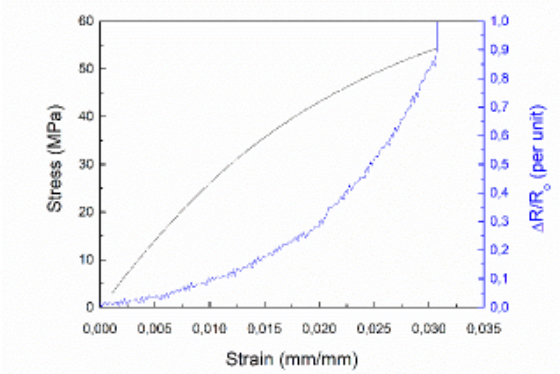
Stress (MPa)
ΔR/R0 (per unit)
Strain (mm/mm)
0,000
0,005
0,010
0,015
0,020
0,025
0,030
0,035

(b)

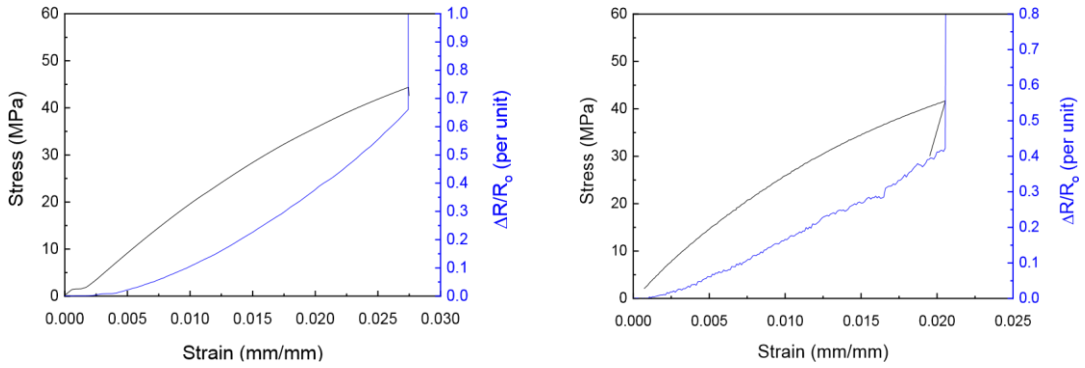

Figure 4.

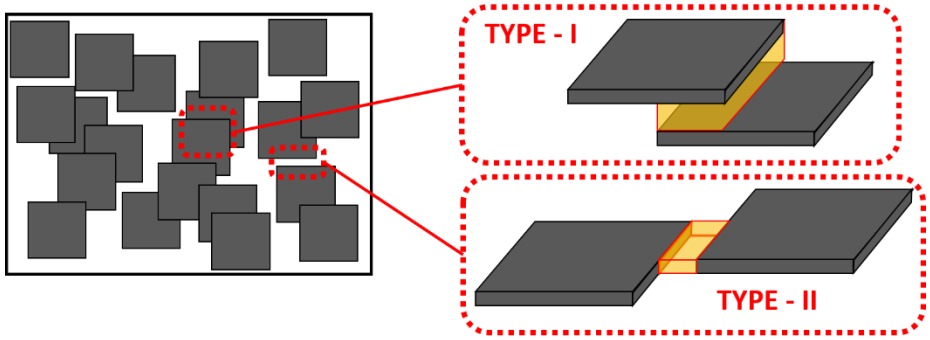

Figure 5.

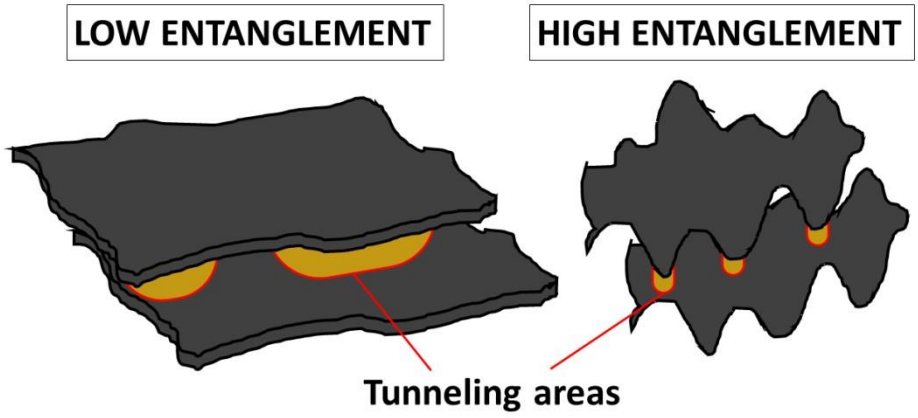

Figure 6.

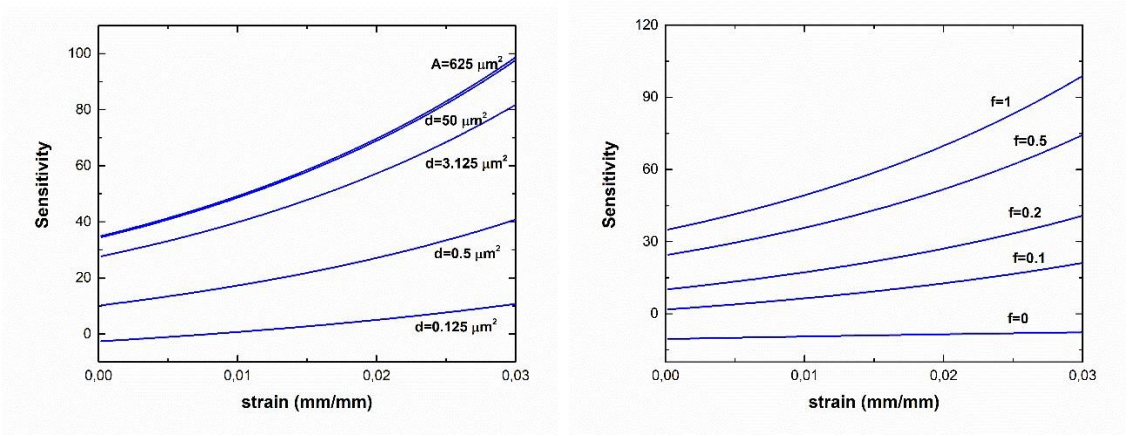

(a) (b)

Figure 7.

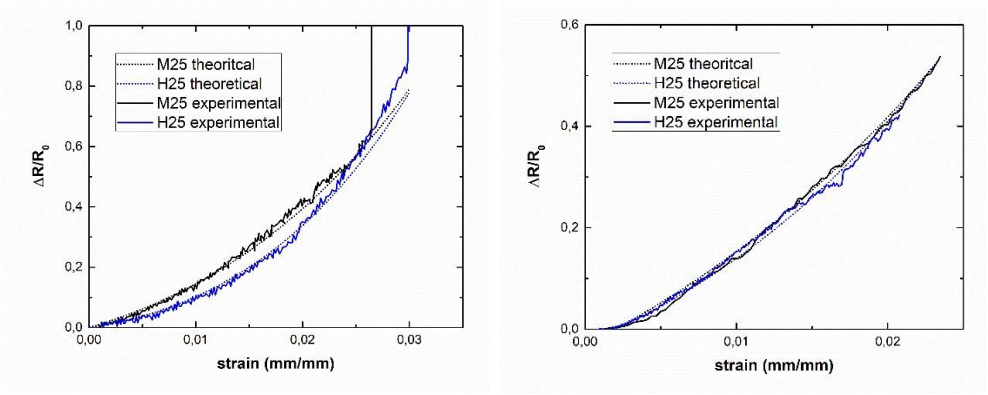

(a) (b)

Figure 8.

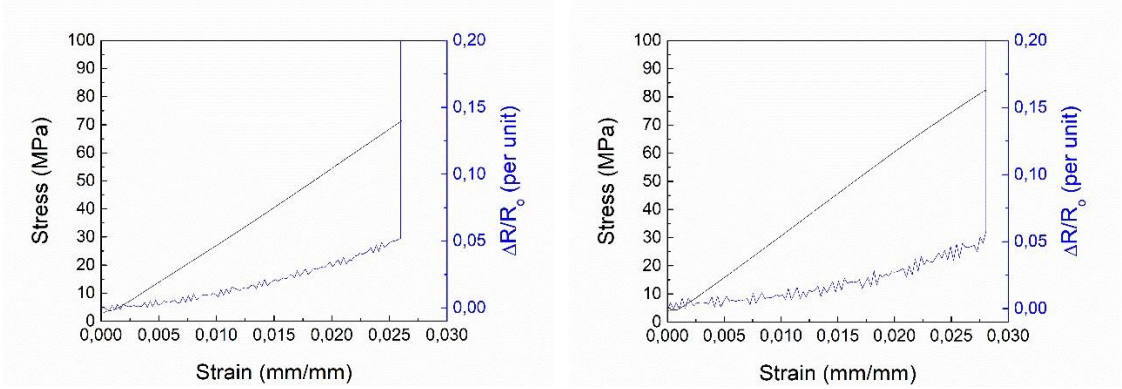

(a) (b)

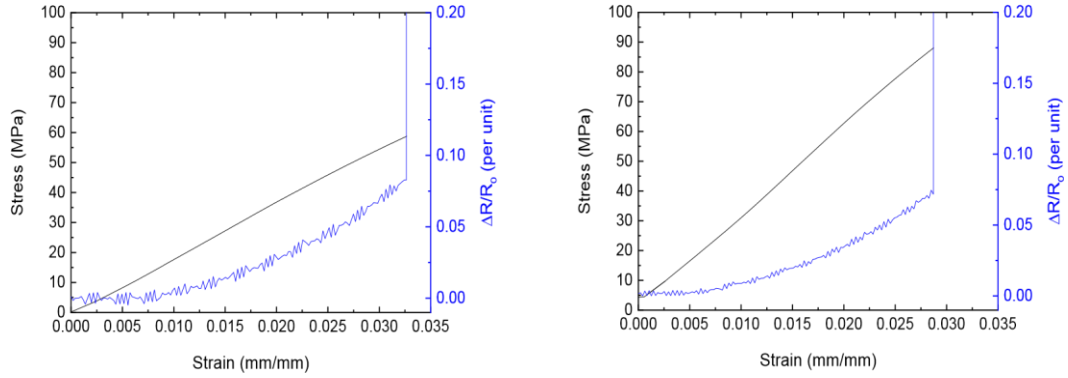

(c) (d)

Figure 9.

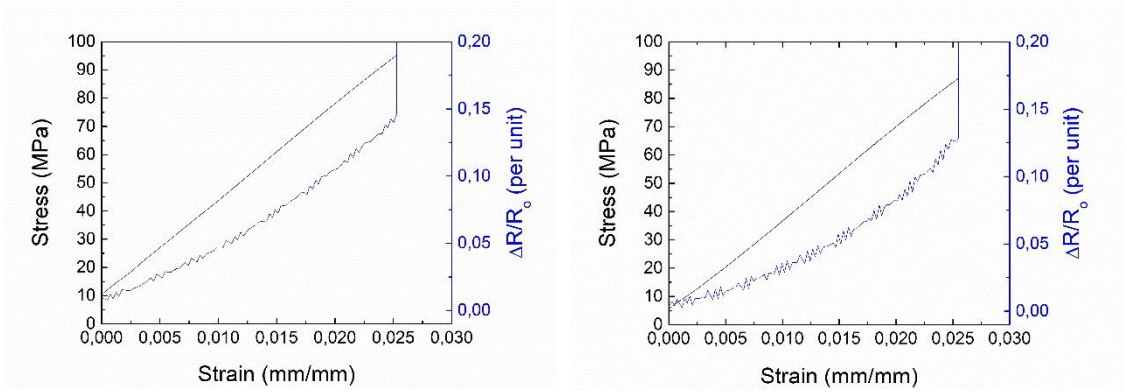

(a) (b)

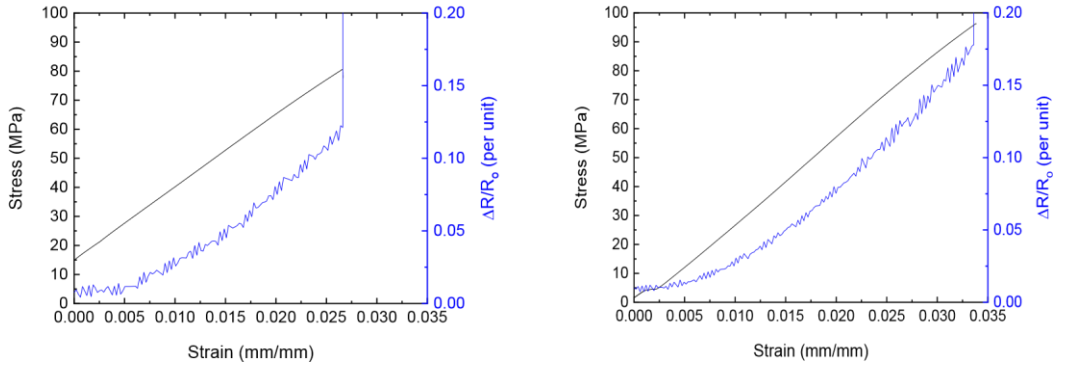

(c) (d)

Figure 10.

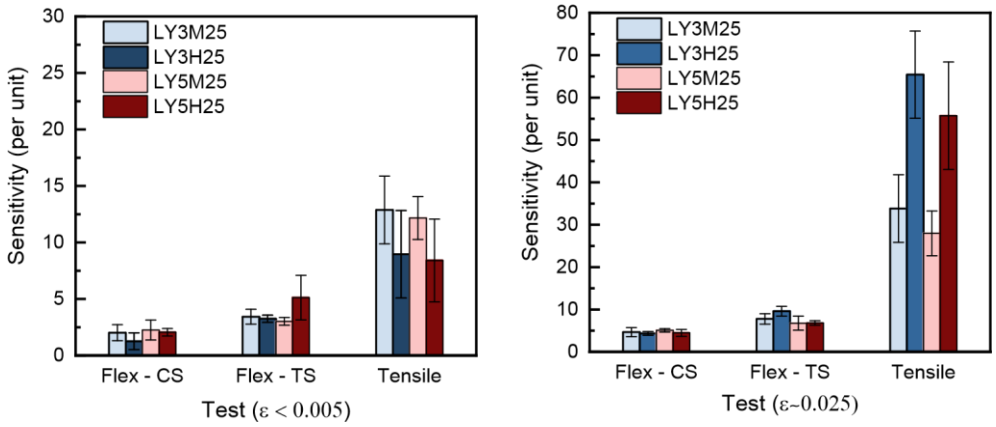
LY3M25
LY3H25
LY5M25
LY5H25
Sensitivity (per unit)
Flex - CS
Flex - TS
Tensile
Test (ε < 0.005)
Test (ε~0.025)

(a) (b)

Figure 11.

TABLES

Table 1. Summary of main properties of M25 and H25 particles

Property	M25	H25
Average diameter (μm)	25	25
Average thickness (nm)	6	15
Oxygen content (%)	<1	<1
Residual acid Content (%)	0.5	0.5
Electrical conductivity (S/m)	10^7 10^2 (out of plane)	10^7 10^2 (out of plane)

Table 2. Conditions used in sonication and calendering processes for dispersion of GNPs in the epoxy resin.

Process	1- Sonication			2- Calendering		
	Amplitude (%)	Cycle (s)	Time (min)	Repetitions	Rollers gap (μm)	Velocity (rpm)
1	50	0.5	45	-	-	-
2-1	-	-	-	1	5 - 5	250
2-2	-	-	-	1	5 - 5	300
2-3	-	-	-	1	5 - 5	350

Table 3. Electrical conductivity values of nanocomposites.

Nanocomposite	Average thickness of GNPs	σ (S/m)
LY3M25	6	$(37 \pm 7) \cdot 10^{-5}$
LY5M25	6	$(25 \pm 8) \cdot 10^{-4}$
LY3H25	15	$(11 \pm 6) \cdot 10^{-4}$
LY5H25	15	$(27 \pm 5) \cdot 10^{-3}$